Process Biochemistry 111 (2021) 167–177

Contents lists available at ScienceDirect

Process Biochemistry

journal homepage: www.elsevier.com/locate/procbio

Plant-derived synthesis and characterization of gold nanoparticles: Investigation of its antioxidant and anticancer activity against human testicular embryonic carcinoma stem cells

Fahimeh Mobaraki [a], Mohsen Momeni [b], Mohammad Ehsan Taghavizadeh Yazdi [c], Zahra Meshkat [d], Mahdi Silanian Toosi [e], Seyed Mousalreza Hosseini [f,g,*]

[a] Department of Anatomy and Cell Biology, School of Medicine, Mashhad University of Medical Sciences, Mashhad, Iran
[b] Immuno-Biochemistry Lab, Immunology Research Center, Mashhad University of Medical Sciences, Mashhad, Iran
[c] Applied Biomedical Research Center, School of Medicine, Mashhad University of Medical Sciences, Mashhad, Iran
[d] Department of Microbiology and Virology, School of Medicine, Mashhad University of Medical Sciences, Mashhad, Iran
[e] Cancer Research Center, Mashhad University of Medical Sciences, Mashhad, Iran
[f] Surgical Oncology Research Center, Mashhad University of Medical Sciences, Mashhad, Iran
[g] Department of Gastroenterology, School of Medicine, Mashhad University of Medical Sciences, Mashhad, Iran

ARTICLE INFO

Keywords:
Achillea biebersteinii
AuNPs
Testicular cancer
NTERA-2 cells
Heat shock proteins
Bax/Bcl2/Caspase gene expression

ABSTRACT

In this unprecedented study, the anticancer properties of gold nanoparticles synthesized using *Achillea biebersteinii* flower extractwere investigated. Nanoparticle synthesis using herbal extracts is low-cost and can, therefore, serve as an economically viable alternative for large-scale nanoparticle production. The smallest nanoparticles were spherical within a range of 2–30 nm (with an average of 8 nm). The gold nanoparticles were characterized using UV-visible spectrophotometry, x-ray diffraction, Fourier-transform infrared spectroscopy, dynamic light scattering, and transmission electron microscopy. The gold nanoparticles displayed great antioxidant potential similar to the positive control. Their cytotoxic effects on human testicular embryonic carcinoma stem cells were assessed using the MTT assay and acridine orange/propidium iodide. The nanoparticles demonstrated dose-dependent cell viability against cancer cells, and the half inhibitory concentration (IC50) values were 10 μg/mL. The expression of Bax, Bcl2, caspase-3, caspase-9, p53, and HSPA2 genes was evaluated using reverse transcription-polymerase chain reaction (RT-PCR) analysis to further confirm that gold nanoparticles induced apoptosis. The cytotoxicity analysis results indicated that the gold nanoparticles were toxic for NTERA-2 cells. These positive outcomes can contribute to the rational design of novel anticancer agents.

1. Introduction

Despite the extensive advances in disease control and treatment, cancer remains a grave global health challenge [1,2] and the second leading cause of death, after cardiovascular disease [3]. Testicular or germ cell carcinoma accounts for about 95 % of all cases of testicular cancer which is the most frequent cancer in men aged 15–35 [4]. Testicular cancer is greatly similar to human embryonic stem cells and, in some cases, its differentiation has been observed in these cells. However, the cell origin of testicular cancer is unknown due to various types of sexual cells in the testicle. Pre-cancerous changes may occur in pre-puberty and even during fetal life; when the cells are mature, they become cancerous by stimulating factors such as hormones [5]. The most common treatment method for all types of cancers is chemotherapy. However, a critical challenge in chemotherapy is acquired resistance to cancer drugs, causing a major problem for cancer treatment [6]. Recently, a crucial strategy leading to the advancement of medical research and the development of new methods against cancer has been the application of nanoparticles to anti-cancer drug targeted delivery [7,8]. The synthesis of metallic nanoparticles derived from noble metals has gained the attention of many researchers due to the nanoparticles' vast applications [9,10]. They are primary particles with at least one dimension of 1–100 nm [11]. Particles at this scale have new properties that can be fundamentally applied to electronics, energy, medical science, biotechnology, and environmental science [12,13].

Among the different types of nanoparticles, metal nanoparticles such

* Corresponding author at: Surgical Oncology Research Center, Mashhad University of Medical Sciences, Mashhad, Iran.
E-mail address: HoseiniMR@mums.ac.ir (S.M. Hosseini).

https://doi.org/10.1016/j.procbio.2021.09.010
Received 18 April 2021; Received in revised form 14 September 2021; Accepted 15 September 2021
Available online 17 September 2021

as gold (AuNPs) and silver nanoparticles (AgNPs) are particularly significant owing to their unique properties [14,15]. AuNPs have been described as rising stars in the field of nanomedicine. AuNPs loaded with plant metabolites have been employed for their antimicrobial, antitumor, anti-inflammatory, and antioxidant characteristics [16]. In addition, AuNPs have displayed potential as antitumor factors for biomaterial delivery [17]. AuNPs confer abundant benefits over other nanomaterials, mainly due to their different sizes, morphologies, and unique physicochemical properties [18,19]. Physical and chemical methods are employed for nanoparticle fabrication. The disadvantages of these methods include high cost and the risk associated with using chemicals that remain in nature, leading to chemical pollution [20]. Other undesirable characteristics of these methods include the low production rate and the use of high pressure, temperature, and energy during the reaction process. Since nanoparticles are highly reactive with biomolecules, stabilizers are added (coating) to maintain their desired properties [21]. Nevertheless, chemical species adsorbed on the particle surface may have adverse biological impacts and be harmful to human health [22].

An environmentally safe method for nanoparticle production is the biological synthesis method [23]. Recently, several researchers have reported nanoparticle biosynthesis using a wide range of bio-resources such as bacteria, fungi, and plants [24,25]. Studies have demonstrated the role of polyphenols, carbohydrates, proteins, and especially plants in the regeneration of metal salts for nanoparticle synthesis [26,27]. Researches have shown that the surface of nanoparticles produced using this method was covered by plant metabolites. Moreover, carbohydrates, proteins, and phenolic compounds made them more biocompatible as well as sustainable. Hence, the application of plants in biotechnology may overcome the obstacles associated with nanoparticle fabrication [28,29]. Gold nanoparticles (AuNPs) have been widely considered for molecular identification, chemical usage, and biomedical applications in recent years owing to their great particular surface area and excellent conductivity [30]. Moreover, AuNPs have a variety of bio-applications that are biocompatible [31]. Plants show a high potential to make nanoparticles, but researchers have yet to identify all the plants possessing this potential [32,33].

In recent years, researchers have reported anti-inflammatory activity, anti-tumor effects, and strong anti-proliferative activity in cancer cells exposed to *Achillea biebersteinii* Afan. extract [34,35]. The presence of major compounds of piperitone, cineole, limonene, and p-cyment in this plant is reported, indicating the presence of four flavonoids, one hydrocarbon, and one alcohol, which are responsible for the exceptional properties of *A. biebersteinii* Afan., also commonly referred to as yarrow [36]. Due to the presence of abundant metabolites and biomolecules in *A. biebersteinii* and the unique properties of AuNPs, in this pioneering study, *A. biebersteinii* flower extract was used for the first time as a reducing and capping agent for AuNP synthesis, and its anticancer effect on human testicular embryonic carcinoma cells (NTERA-2) was evaluated.

2. Experimental procedure

2.1. Materials, reagents, and plant extract preparation

Fresh *A. biebersteinii* Afan. plant was collected from the north of Khorasan-Razavi Province, Iran. The plant species was identified and coded in the botanical herbarium of the Ferdowsi University of Mashhad (FUMH code: 27797) and had the genetic code NCBI: txid282722. The yarrow flowers were thoroughly washed with deionized water and then placed at room temperature to dry under dust-free conditions in the shade. The dried flowers were then powdered for extraction. Next, 15 g of powder was mixed with 100 cc of deionized water and placed on a magnetic heater-stirrer for 15 min to boil. The mixture was filtered after it cooled using a Whatman paper and stored at 4 °C for subsequent experiments. This solution was considered as the base extract (100 % extract) and the other concentrations were made from it. Gold salt ($HAuCl_4.3H_2O$, 99.9 %) and other chemical materials were procured from Merck Company (Germany).

2.2. AuNP fabrication using plant extract

The plant extract and gold chloride solution ($AuCl_4$) (1 mM) were mixed at the ratios of 9:1 (90 mL extract/10 mL $HAuCl_4$), 8:2 (80 mL extract/20 mL $HAuCl_4$), and 7:3 (70 mL extract/30 mL $HAuCl_4$). The colloidal solutions were placed on the magnetic heater-stirrer and then controlled at different temperatures (25, 40, and 80 °C) at various time intervals (30, 60, 120, and 240 min).

2.3. Characterization of biosynthesized AuNPs

Preliminary characterization and absorption spectra were measured using a spectrophotometer (Shimadzu UV-2500 model, Japan) tested in the range of 400−700 nm. The AuNP mixture was centrifuged (14,000 rpm) for 10 min and washed with sterile deionized water; then, the superfluous solution and impurities were discarded and the nanoparticle powder was obtained by the freeze-drying method. To prepare the XRD pattern, a powder diffractometer (Philips X'pert Pro model, the Netherlands, Amsterdam) was constructed using a Cu Kα copper anode source with a wavelength of $\lambda = 1.5406$ A°. The X-ray diffraction technique was applied to test the structure, metal nature, and elemental composition of the Ab-AuNPs. To identify biologically active groups involved in the formation of AuNPs, the FT-IR (NICOLET IR 100, USA) was used, and the spectra were evaluated in the range of 500–4000 cm^{-1}. The size distribution profile of the Ab-AuNPs was analyzed by DLS (Photal, Otsuka Electronics Co., Osaka, Japan). The Ab-AuNPs' shape, morphological details, dispersal, and size were analyzed using TEM (Leo 912AB Ab Omega, Zeiss, Germany) operated at 120 kV. Subsequently, the size distribution and image analyses were performed using Image J.

2.4. Antioxidant activity

2.4.1. DPPH free radical scavenging assay

The 2, 2-Diphenyl-1-picrylhydrazyl radical scavenging analysis for Ab-AuNPs was performed as explained by the standard method [37]. In this assay, each sample solution was diluted in water, and the final concentration of the extract and Ab-AuNPs was obtained (10–500 μg/mL). Subsequently, 1 mL of the DPPH solution (0.3 mM) was added to 2.5 mL of the sample solution. The values were calculated after 30 min at 518 nm and converted to an antioxidant percentage. The plant extract solution was used as the blank. The negative control was the DPPH solution, and ascorbic acid (routine) was employed as the positive control.

The final percentage was calculated using the following formula [38]:

$$\text{Percentage of inhibition} = \frac{\text{Absorption control} - \text{Absorption test}}{\text{Absorption control}} \times 100$$

2.4.2. SRSA assay

Superoxide radical scavenging activity was assessed using the spectrophotometric measurement of the reduced NBT product, based on the method explained by Nishikimi et al. [39]. The extract and Ab-AuNPs were used in the concentration range of 10–500 μg/mL as a standard. The mixture in a total volume containing the diluted solution sample with water, PMS (0.2 mL, 60 kmol/L, NBT (0.2 mL, 144 kmol/L), and NADH (0.2 mL, 677 kmol/L) in phosphate buffer was incubated at 25 °C for 5 min [38]. The absorbance (Ab) of formazan chromophore was read by spectrophotometry (BioTek, Epoch, USA) at 560 nm. The tests were performed in triplicate and averaged.

2.5. Cell culture and cell toxicity of Ab-AuNPs

The human testicular embryonic carcinoma stem cells (NTERA-2 cell line) were obtained from the Iranian National and Genetic Reserves Cell Bank (accession cell no: IBRC C10509). The cells were cultured in a culture medium of DMEM +2 mM L-Glutamine + 15 % FBS and subculture (split subconfluent cultures, 70–80 %), using 0.25 % trypsin, 0.02 % EDTA, and incubated at 37 °C with 5% CO_2 [40]. The cells were evaluated for their number, morphology, and vitality under an introspective microscope. When the cells reached at least 70 % cell growth, they were detached by 5% trypsin and centrifuged at 1500 rpm for 5 min. The resulting cell suspension was established as a suspension, and the cell percentage was specified using a Neubauer slide and trypan-blue dye under a light microscope (Nikon Optiphot, Nikon USA, Melville, NY). To validate non-contamination, cells with a higher percentage (90 %) were used for testing. The *in vitro* cytotoxicity of Ab-AuNPs on the NTERA-2 cell line was studied using the MTT assay. The cells were seeded into 96-well plates (1×10^5 *cell/mL*, NEST®, New Jersey, USA) and treated with diverse concentrations of Ab-AuNPs (0, 0.5, 1.5, 3, 6, 12, 25, 50, and 100 μg/mL) for 24 h. Afterward, 20 μL of the MTT solution (Merck, Germany) was added to each well and incubated for 2 h at 37 °C. At the end of the incubations, 100 μL (DMSO) was added to dissolve formazan crystals for four hours in a dark environment. The violet crystals of formazan formed in the surviving cells were dissolved, and a colorless liquid was uniformly produced. The absorbance of each well was read at 570 nm after 30 min of incubation using a plate reader and microplate spectrophotometer (Biotek Epoch, USA). The results were described as the IC50 percentage (concentration that inhibits cell growth up to 50 %). To achieve an improved result, the trials were performed in triplicate, and the percentage of viable cells was calculated according to the following formula [41]:

$$\text{Percentage of cell vitality } (\%) = \frac{\text{Mean absorbance of the treated sample}}{\text{Mean absorbance of the control sample}} \times 100$$

2.6. Apoptosis detection by acridine orange and propidium iodide (AO/PI)

The effects of apoptosis induction on Ab-AuNPs-treated NTERA-2 cells were measured using the AO/PI test [42,43]. Briefly, the treatment was performed on a 6-well microplate. The NTERA-2 cells were plated at a concentration of 1×10^6 cells/mL and treated with Ab-AuNPs at 0, 10, 25 μg/mL concentrations. The cells were incubated at 37 °C for 24 h. The supernatant was discarded, and the cells were washed twice with PBS. Fluorescent dyes having AO (10 μg/mL) and PI (10 μg/mL) were added to the cellular pellet at the same volumes. After 3−5 min, 100 mL of the supernatant was removed and placed on the slide of the Neubauer rhodium hemocytometer. Apoptotic cell percentage was assessed under a fluorescent microscope (Olympus CKX41, Tokyo, Japan) and measured by the following formula [43]:

$$\text{Percentage of total apoptotic cells } (\%) = \frac{\text{Total number of apoptotic cells}}{\text{Total number of apoptotic and normal cells}} \times 100$$

2.7. RNA isolation and gene expression by real-time PCR (RT-PCR)

A standard method was employed for this part of the study [44]. NTERA-2 cells were cultured separately in two cell culture flasks. One of them was incubated with the Ab-AuNPs at (IC50) for 24 h, and the others without treatment were evaluated as controls. Then, the cells were trypsinized and centrifuged. The entire RNA of the treated cells was isolated according to the protocol by a High Pure RNA isolation kit (Qiagen, Hilden, Germany). The extracted RNA was treated with DNase I to prevent DNA contamination. To prepare cDNA with oligo (dT), a first-strand complementary synthesis kit was used based on the manufacturer's protocol (Fermentas, Lithuania). To perform the qualitative PCR steps, specific primers (Table 1) and a mixer containing SYBER Green (GENET BIO, Korea) were used. For gene expression levels, the 40-step cycle was performed by a Light Cycler® 96 Real-Time PCR System thermocycler (Roche, Germany). Gene expression changes were measured using the 2-ΔΔCt method. The test was performed in triplicate and the optimal thermal profile for BCL2, BAX, CASPASE-3, CASPASE-9, P53, and HSPA2 included a primary denaturation step at 95 °C (10 min), followed by 45 cycles at 94 °C (30 s), particular annealing temperature (30 s), and 72 °C (30 s).

2.8. Data analysis

The quantitative data were analyzed using one-way analysis of variance (ANOVA) and Tukey's test for multiple comparisons as a posttest in SPSS 22. The results are presented as mean ± SD and the significance level is p-value <0.05. The $\chi 2$ or Fisher's exact test and Pearson's correlation analysis were performed to evaluate the association between gene expressions. Finally, the graphs were plotted in Microsoft Excel.

3. Results and discussion

3.1. Characterization of Ab-AuNPs

3.1.1. UV–vis spectrophotometry

Ab-AuNPs synthesis was performed using the aqueous flower extract of the *A. biebersteinii* Afan. UV–vis spectroscopy was employed to specify the optical properties of the biofabricated AuNPs. Ab-AuNPs have sharp surface plasmon resonance (SPR) absorption, which is influenced by the fabricated nanoparticles' morphology and nature [45]. The wavelength was measured in the range of 400–700 nm. The distinctive absorption peak at 540 nm confirmed the formation of Ab-AuNPs. The appearance of a violet color following the mixture of the extract with $AuCl_4$ solution indicated the creation of AuNPs [46]. The reaction mixture color change from green to dark purple was noticeable (Fig. 1). This color change was attributed to a redox reaction, which was the reduction of Au (III) to Au (0) by biomolecules existing in the extract [47].

The fabricated nanoparticles' spectra were monitored by UV–vis spectroscopy at different extract and gold salt contents, temperatures, and times [48]. The absorption curve was observed in all the conditions; however, the strongest and most symmetrical absorption peak belonged to the high ratio of extract concentration to chloroauric acid 9:1 (90 mL extract/10 mL $HAuCl_4$) at 80 °C within 2 h, and the absorption peaks were stable over time (Fig. 2). The spectrum patterns showed that the lowest reaction rate and the weakest absorption peak for the synthesis of gold nanoparticles were 7:3 (70 mL extract/30 mL $HAuCl_4$) at 25 °C (Fig. 2). Sung et al. reported an upward linear relationship between nanoparticle formation and its absorption peak at different times such that, during a certain time, as the concentration of nanoparticles increased, its absorption peak also increased and then stopped [49]. In

Table 1
Primer sequences of apoptotic gene expression.

	Gene	Forward Primer	Reverse Primer	Annealing	Product size (bp)
1	BCL2	5′ CAGGATAACGGAGGCTGGGATG 3′	5′ GACTTCACTTGTGGCCCAGAT 3′	59	157
2	BAX	5′ CCCTTTTGCTTCAGGGTTTCAT 3′	5′ TCAGCTGCCACTCGGAAAAA 3′	59	223
3	CASPASE3	5′ ACTGGACTGTGGCATTGAG 3′	GAGCCATCCTTTGAATTTCGC 3′ 5′	60	138
4	CASPASE9	5′ CGGTGACCCCAGAATTGACC 3′	5′ CCTGCCCGCTCACGTC 3′	61	164
5	P53	5′ TGCTCAAGACTGGCGCTAAA 3′	5′ CAGTCTGGCTGCCAATCCA 3′	59	157
6	HSPA2	5′ TTGCAACCCCATCATCAGCA 3′	5′ TTGGCACAAGGACATTTCAAAGA 3′	59	192
7	GAPDH	5′ GGAAGGTGAAGGTCGGAGTCA 3′	5′ GTCATTGATGGCAACAATATCCACT 3′	58	101

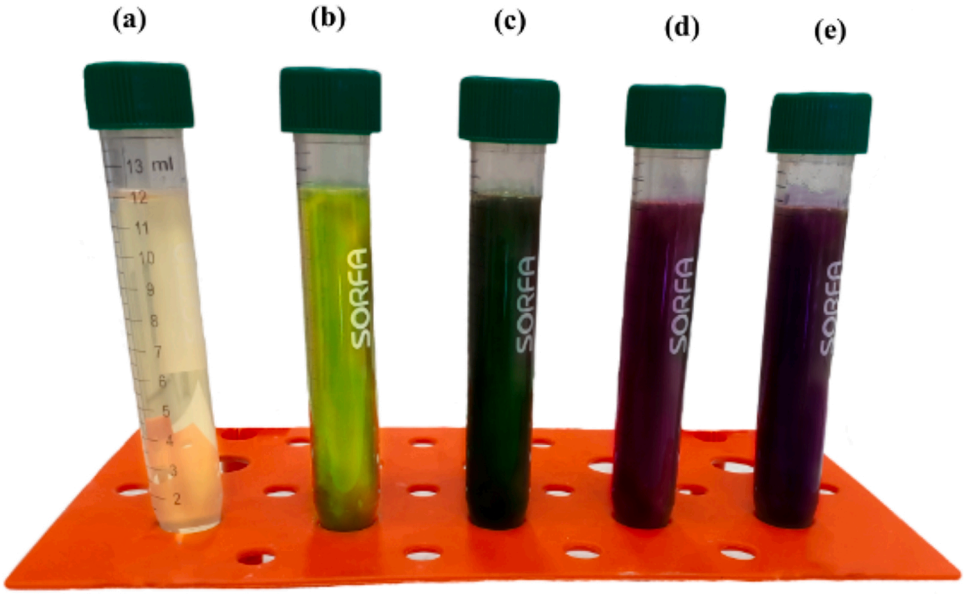

Fig. 1. The reaction solution of mixing the aqueous flower extract of *A. biebersteinii* with the $HAuCl_4$ solution. (a) 1 mM $HAuCl_4$ solution; (b) plant extract; (c) The color of the reaction solution changes to dark green after 30 min; (d) The color changed to purple after 1 h; (e) The color changed to dark purple after 2 h.

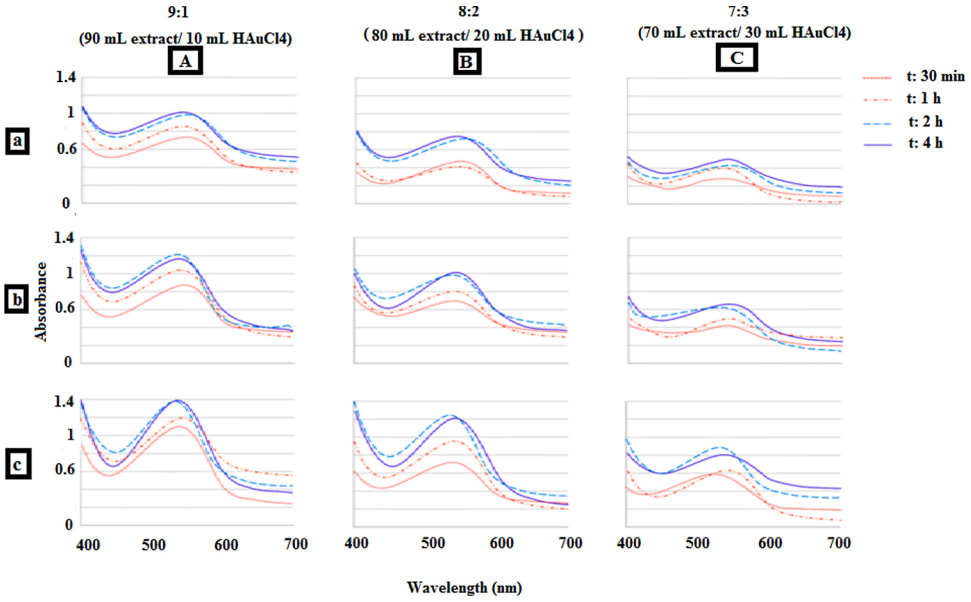

Fig. 2. UV–vis spectra of Ab-AuNPs at different extract concentrations at various ratios of (A) 9:1; (B) 8:2; (C) 7:3. At each reaction ratio of the extract and $HAuCl_4$, different temperatures are shown (a) 25 °C; (b) 40 °C; (c) 80 °C.

the Ab-AuNP synthesis, the presence of the most intense and symmetric absorption peak indicated the highest nanoparticle concentration [50, 51]. In general, the initial delay in the formation of gold nuclei decreased with increasing the temperature and plant extract concentration. These results are in line with the findings of other researchers [49]. Many studies reported a relationship between raising the reaction

speed and increasing both the reaction temperature and the plant extract concentration in gold nanoparticle synthesis [49–52]. Furthermore, in some samples, the absorption peaks shifted to longer wavelengths after some time and the reaction continued; or due to the accumulation or deposition of the produced nanoparticles, their absorption intensity was decreased. Khalil et al. reported that in green nanoparticle synthesis, over time, the absorption peaks shifted to longer wavelengths due to the continued reduction of the secondarily formed nanoparticles and their enlargement [53].

3.1.2. FTIR

FT-IR spectroscopy is a typical method to identify the functional groups of different compounds [54]. The nature of regenerative biomolecules in the formation of Ab-AuNPs and the bioactive components of the extract was studied by FTIR spectroscopy and compared. The FTIR spectra of Ab-AuNPs and flower extract are displayed in Fig. 3. Band 2921 could be related to the C—H stretch fluctuations of the carbon chain, and the 1865 band could be related to the stretch oscillations of the C—O amino acids [55]. Band 1535 belonged to C═C groups in aromatic rings. Band 1455 was attributed to the CH—CH bond in the sugars or lipids in the extract [56]. Band 1110 belonged to the stretch oscillations in the first-type alcohols or the C—N in the aliphatic amines. The 794 band was related to the C—H bond of aldehydes or halogen compounds such as chlorides and bromides [55]. According to the FT-IR results, a similarity was observed in the Ab-AuNPs and extract with different intensities (Fig. 3), which could confirm the biosynthesis of Ab-AuNPs. The presence of a new bond in 1730 in the spectrum after gold ion resuscitation was attributed to the stretch oscillations of the C═O functional group of carbonyl or carboxylic acid compounds [55, 56]; the spectra revealed that polyols were generally accountable for the reduction and stabilization of gold ions, whereby they were oxidized to unsaturated carbonyl groups and led to the mentioned peaks [57]. The slight drift detected in the intensity of the FTIR spectra of the extract and the Ab-AuNPs could be due to phytochemical ligands with the metal surface [58]. The FTIR results indicated the role of proteins and other functional groups in the biosynthesized AuNPs' reduction, capping, and stabilization.

3.1.3. X-ray diffraction (XRD) analysis

The XRD pattern of the dried powder of the prepared Ab-AuNPs is illustrated in Fig. 4. The XRD peaks are located at angles 38.16 °, 44.43 °, 64.67 °, 77.64 °, and 44.43 °, corresponding to 111, 200, 220, and 311 planes of Ab-AuNPs [59,60]. During the comparison, the graph obtained from the biosynthesized Ab-AuNPs by the gold standard chart showed that both graphs match [61]. Thus, it was ensured that the produced nanoparticles were gold nanocrystals. The presence of strong peaks in the patterns displayed a great degree of crystallinity for nanoparticles [62]. These results were in agreement with the database of the Joint Committee on Powder Diff ;raction Standards (JCPDS, No

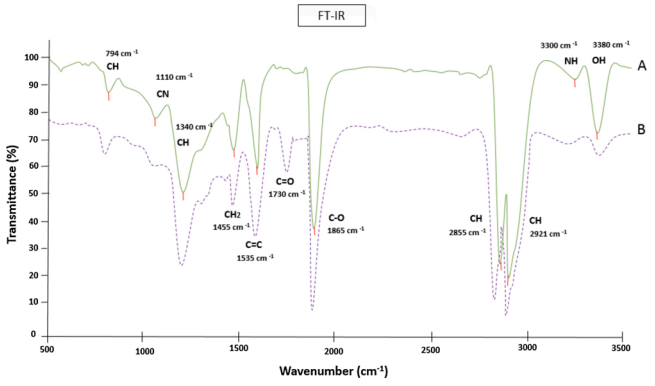

Fig. 3. FTIR spectra of (A) *A. biebersteinii* flower extract; (B) Ab-AuNPs.

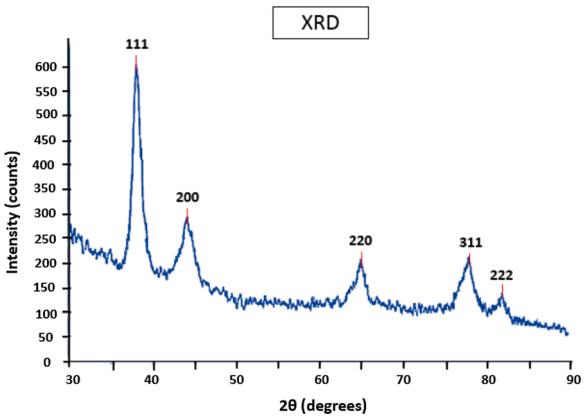

Fig. 4. XRD pattern of the biosynthesized Ab-AuNPs. The XRD peaks are placed at angles of 38.16 °, 44.43 °, 64.67 °, 77.64 °, and 44.43 ° corresponding to 111, 200, 220, and 311 planes of Ab-AuNPs.

04-0784). The reported peak values also matched the XRD patterns of AuNPs obtained by various green synthesis methods [63].

3.1.4. TEM and DLS studies

The size and morphology of the biosynthesized nanoparticles with a ratio of 9:1 (90 mL extract/10 mL $HAuCl_4$) and the highest peak and absorption peak in UV–vis spectroscopy were observed at three temperatures (25 °C, 40 °C, and 80 °C) using TEM, and the size distribution of Ab-AuNPs was assessed using DLS. As the reaction temperature increased, the synthesized nanoparticles' size decreased; the average size of Ab-AuNPs decreased from 48 nm to 8 nm by increasing the temperature from 25 °C to 80 °C (Fig. 5). Song et al. (2009) reported that in the fabrication of AuNPs using magnolia plant extract, by increasing the reaction temperature from 25 °C to 95 °C, the mean diameter of the nanoparticles decreased from 110 nm to 40 nm [49]. The Ab-AuNP size reduction could be due to the rise in reaction temperature and, after that, the increase in reaction rate. Therefore, most of the gold ions were involved in the formation and consumption of the particles' primary nuclei; consequently, the secondary resuscitation process on the primary nucleus was stopped, and the secondary growth of the particles was dramatically reduced [64]. DLS analysis revealed that, as the temperature increased, the size distribution of Ab-AuNPs became more uniform, which is also confirmed by TEM as a powerful and unique tool for structure and shape characterization [65]. The TEM images of the nanoparticles were clearly separated, indicating that their dispersion index was appropriate. Hence, the size distribution of the nanoparticles formed by the ratio of 9:1 at 80 °C was relatively uniform, and the particles were mostly the same size, and their dispersion range was about 2–30 nm, with an average size of 8 nm. On the other hand, the particles formed with the same ratio of plant extract and gold salt at 25 °C had different sizes (10−70 nm). The TEM images demonstrated that the nanoparticles were predominantly of a spherical shape. In a similar study, the TEM analysis of AuNPs by chitosan showed that nanoparticle size was 10–50 nm, and various shapes, including spherical, were visible [66]. Andeani et al. described the synthesis of AuNPs by a species of yarrow plant (*Achillea wilhemsii*) with spherical shapes. In this study, DLS and TEM results confirmed, via UV–vis spectroscopy, that significant differences in nanoparticle size could be due to the uptake of macromolecules (proteins, polysaccharides, etc.) and highly hydrophilic compounds on the nanoparticles' surface, resulting in a high volume of nanoparticles. Therefore, in the DLS technique, the hydrodynamic radius of the nanoparticles increased [67]. Huang et al. also reported that smaller nanoparticles could penetrate deeper and localize into tumor cells. They found that ultra-small Ab-AuNPs of sizes 2 and 6 nm accumulated at high levels in mice tumor tissues. These nanoparticles were also distributed in the nucleus and throughout the

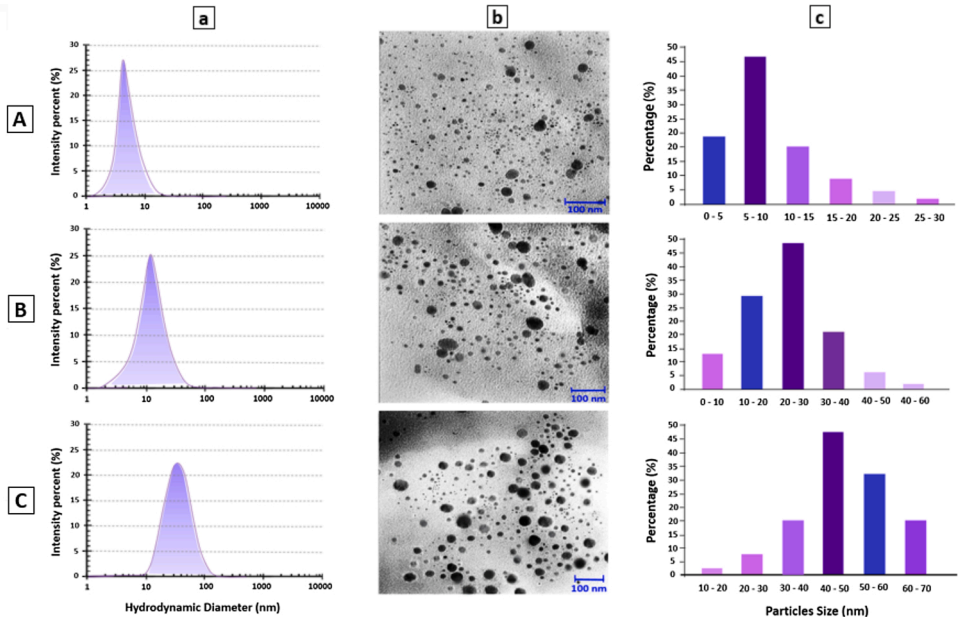

Fig. 5. Size histograms of Ab-AuNPs at different temperatures. (A) 25 °C, (B) 40 °C, and (C) 80 °C by (a) DLS; (b) TEM images, and (c) particle size distribution. By raising the reaction temperature from 25 °C to 80 °C, the nanoparticle size decreased, and the average size of Ab-AuNPs was reduced from 48 nm to 8 nm.

cytoplasm of cancer cells both *in vitro* and *in vivo*, although AuNPs with a size of 15 nm were found only in the cytoplasm of the cancer cells [68]. In this research, Ab-AuNPs with an average size of 8 nm were utilized to investigate antioxidant activity and anti-cancer effects on cancer cells.

3.2. Antioxidant activity of biosynthesized gold nanoparticles (Ab-AuNPs)

The antioxidant activity of Ab-AuNPs was also evaluated by the DPPH scavenging test with rutin as a positive control. The DPPH assay is a rapid way to evaluate the free-radical quenching capability of compounds and can be stabilized when it accepts electrons [69]. Herein, the dose-dependent DPPH scavenging property of both *A. biebersteinii* flower extract and Ab-AuNPs was found to intensify with enhancing concentrations, and at higher concentrations, both of them exhibited better DPPH scavenging activity than rutin (Fig. 6A). The IC50 values of the plant extract, AuNPs, and rutin were 382.56, 261.84, and 147.93 μg/mL, respectively. The Ab-AuNPs were found to be effective against the DPPH radicals. They also displayed superior DPPH scavenging activity compared to the plant extract. A recent study has reported a similar antioxidant capacity for AuNPs using *Allium sativum* L. leaf aqueous extract which had excellent potential for DPPH inhibition at the IC50 value of 231 μg/mL [70].

Similar observations on increased DPPH scavenging activity with AuNPs fabricated from *Gymnema sylvestre* leaf extract (GYLE) were reported by Nakkala et al. It was shown that GYAuNPs had better

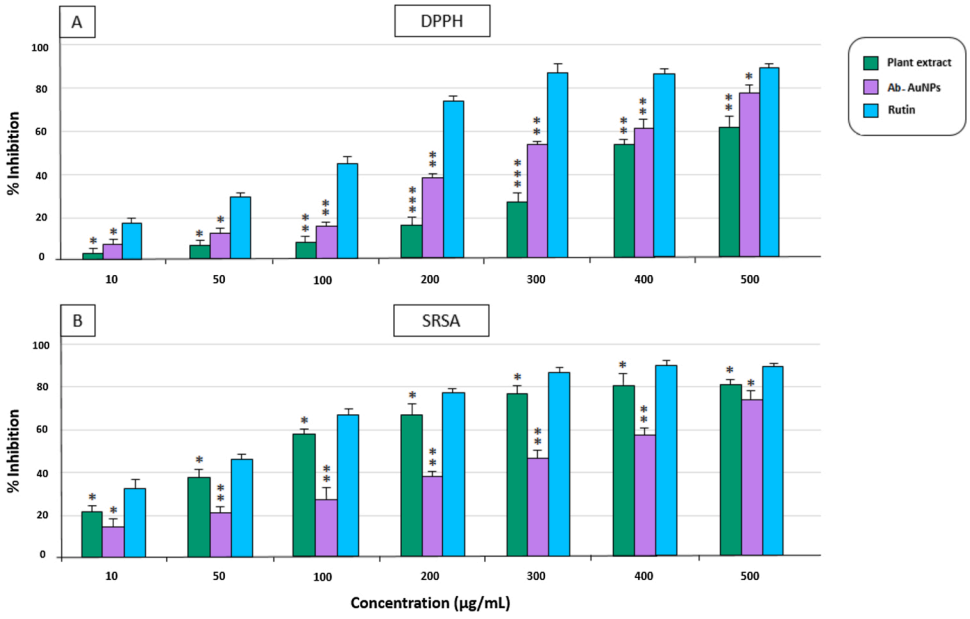

Fig. 6. Antioxidant scavenging activities of *A. biebersteinii* extract and Ab-AuNPs. (A) DPPH radical scavenging activity, (B) superoxide scavenging activity. Values are shown as mean ± SD of triplicate analysis (n = 3). The bar graphs with asterisks denote a significant difference $*p < 0.05$, $**p < 0.01$ and $***p < 0.001$ versus control (rutin).

antioxidant properties than GYLE at different concentrations [71].

The superoxide radical activity of the extract and Ab-AuNPs was examined by the PMS–NBT reduction system. Plant extract and Ab-AuNPs showed outstanding superoxide radical reducing properties, with an effect comparable to that of standard antioxidant rutin (Fig. 6B). Both the extract and NPs demonstrated enhancing activity with a larger concentration, and the reticence percentage caused by the extract and Ab-AuNPs was at 500 μg/mL compared to the antioxidant rutin. Herein, the IC50 values of the plant extract, Ab-AuNPs, and rutin were 78.91, 331.47, and 67.77 μg/mL, respectively. The superoxide scavenging activity of Ab-AuNPs which is increased by raising the concentration and rate inhibition was also demonstrated.

These findings are consistent with the study by Nakkala et al. reporting that biosynthesized GYAuNPs exhibited substantial radical quenching activity comparable to the standard antioxidant rutin [71].

3.3. Antiproliferative activity of Ab-AuNPs against NTERA-2

The MTT test is a common colorimetric method adopted to determine cytotoxicity and measure cell proliferation. Different concentrations of Ab-AuNPs (0, 0.5, 1.5, 3, 6, 12, 25, 50, and 100 μg/mL) were employed to test stem cell viability (NTERA-2) after 24 h, and toxicity was measured by the MTT assay. Based on Fig. 7, untreated cells (control) did not show toxic effects in the test. At 0.5, 1.5, and 3 μg/mL concentrations, Ab-AuNPs displayed less toxic effects than the other treated cells, which were not significant compared to control cells. Nevertheless, the first significant dose of nanoparticles occurred at a concentration of 6 μg/mL with a statistically significant level ($p < 0.05$). Ab-AuNP-treated cells revealed <50 % viable cells at a 12 μg/mL concentration ($p < 0.01$). Hence, inhibitory concentration (IC50) values were calculated and were found to be 10 μg/mL of Ab-AuNPs on NTERA-2 cells. A significant reduction was observed in cell viability by ~50 % compared to the control ($p < 0.01$). The treated cells displayed a little higher toxicity than the Ab-AuNPs at 25 and 50 μg/mL concentrations, which were statically significant compared to the control cells ($p < 0.001$). Further, at the maximum concentration (100 μg/mL), cell viability was 11.5 % in the treated cells, which were statically significant compared to the control ($p < 0.001$) (Fig. 7). When the cells were treated with Ab-AuNPs, the viability of the cells was perpetually decreased in a dose-dependent manner. The outcomes of this study suggest that the cytotoxicity of Ab-AuNPs was enhanced by elevating the NP concentration. AuNPs are found to display potent cell toxicity due to the generation of reactive oxygen species (ROS) leading to cell destruction [72]. Some other investigations on AuNPs also proved their potent cell toxicity towards several cell lines [73,74]. A previous study showed biosynthesized AuNPs with sizes around 10–30 nm by the leaf extract of *Sasa borealis,* indicating cytotoxic effects on AGS cells (gastric cancer). It was reported that cytotoxicity depended on the nanoparticles' size and concentration [75]. In another study, biosynthesis of AuNPs using *Curcumae kwangsiensis folium* leaf aqueous extract with an average size of 16.6 nm had significant efficacy on common ovarian cancer cell lines (SK-OV-3, SW-626, and PA-1). The viability of cancer cells was reduced dose-dependently in the presence of AuNPs [76]. Shuiqin Li et al. fabricated gold nanoparticles using *Mentha longifolia* leaf and investigated the cytotoxicity properties on different cell lines of breast carcinoma (MCF7, Hs 578Bst, Hs 319.T and UACC-3133). They reported that AuNPs acquired anticancer properties for cancer cell removal in a dose-dependent manner [77].

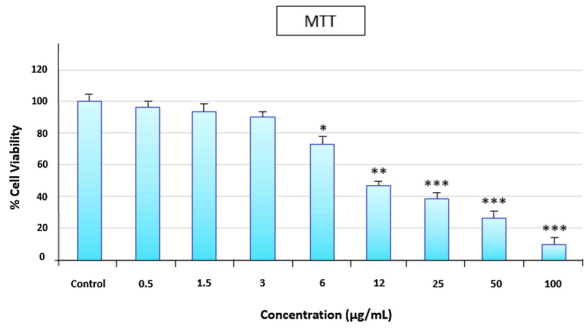

Fig. 7. Cytotoxic analysis of Ab-AuNPs on NTERA-2 cell lines. Cells were treated with Ab-AuNPs for 24 h and cell viability was determined by MTT assay. Error bars represent the mean ± SD of three independent experiments (n = 3). $*p < 0.05$, $**p < 0.01$ and $***p < 0.001$ versus control (untreated group).

Krishnaraj et al. reported that AuNPs and AgNPs reduced the vitality of breast cancer cells in a dose-dependent manner [78]. Based on these investigations, the cytotoxicity of nanoparticles may rely on the size of particles and the nature of cell types. Numerous researchers have drawn similar conclusions [79].

3.4. Apoptosis assay using AO and PI double-staining

In this staining, the green cells with diffused chromatin were viable, and orange cells with condensed chromatin were apoptotic. A total of 100 cells were counted randomly, and the two samples of control and treated cells were compared. In cells treated with Ab-AuNPs (10 μg/mL and 25 μg/mL), the percentage of early apoptotic (orange-green), late apoptotic (dark orange), and necrotic cells (bright red) significantly increased compared to the control sample (Fig. 8). Cell counts showed that Ab-AuNPs triggered morphologic changes in the treated NTERA-2 cells, representing the possible stimulation of apoptosis and necrosis upon treatment in a dose-dependent manner.

The percentage of apoptotic and necrotic cell populations in the treatment groups (B and C) was 53 % and 64 %, respectively ($p < 0.01$, $p < 0.01$), while this percentage was <4% in the untreated cell population of the total cells (Fig. 9). By increasing the concentration of nanoparticles from 10 μg/mL to 25 μg/mL, the apoptotic cell community was decreased to 11 %, while the necrotic cells increased to 24 % ($p < 0.05$). This may have been caused by the development of apoptotic cells into necrotic cells after a particular time. Consequently, necrosis is a post-apoptotic occurrence. This mechanism is visible in cells that are enduring cell death by apoptosis *in vitro*, as an example, by the lack of survival agent signs or activation of multiple death receptors by totally diverse deadly signals. In the absence of phagocytic cells, these cells eventually cease to be metabolically responsive, losing membrane integrity and releasing their cytoplasmic components into the culture medium [80]. These results are in line with those of previous MTT investigations. Wang et al. focused on the biosynthesis of AuNPs using *Scutellaria barbata*. In this report, acridine orange (AO) and propidium iodide (PI) revealed apoptosis-induced morphological in pancreatic cancer cells (PANC-1), confirming apoptotic characteristics at doses of 25 μg/mL and 50 μg/mL [81]. In another study, acridine orange staining demonstrated that the AuNPs synthesized using *Zataria multiflora* leaves altered the Hela cancer cell nucleus and increased apoptotic and necrotic cells [41]. Vairavel et al. also reported that *Enterococcus*-mediated AuNPs at concentrations of 12 and 24 μg/mL in the human colorectal cancer cell line (HT-29) induced apoptosis-associated morphological alterations. The staining results showed early and late apoptotic cells stained with yellowish-green and red dyes, respectively, and that the number of apoptotic cells was increased in a concentration-dependent manner [82].

3.5. Investigation of apoptosis gene expression by RT-PCR

In this experimental study, quantitative real-time PCR was employed to study the gene expression of apoptotic markers (i.e., Bax, Bcl2, caspase-3, and caspase-9) and other related genes, p53 and HSPA2, in untreated NTERA-2 cells by Ab-AuNPs at a concentration of 10 μg/mL for 24 h (IC50). Overall, cancer occurs after some alterations, such as

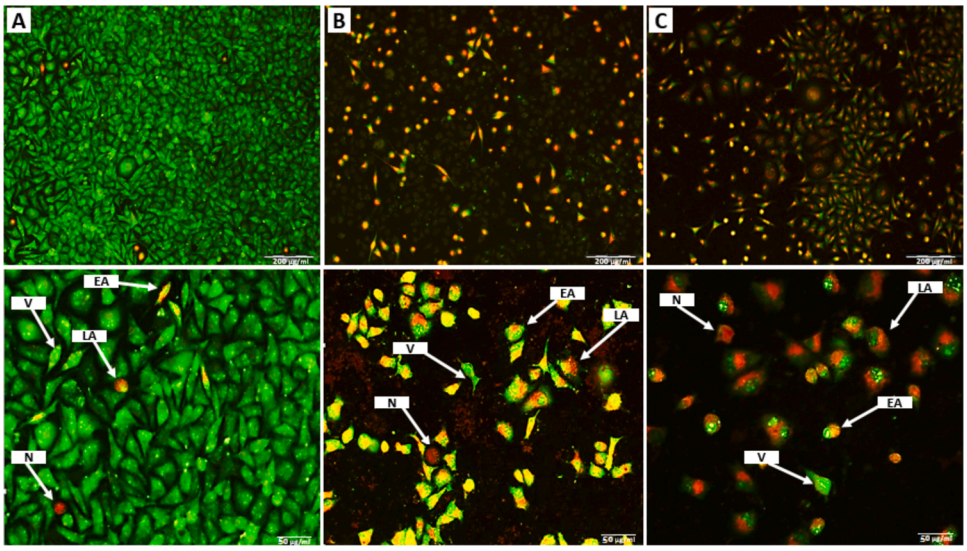

Fig. 8. Fluorescent micrograph of AO/PI double-stained NTERA-2 cells. Cells were treated with concentrations of A) 0, B) 10, and C) 25 μg/mL of Ab-AuNPs. (A): Most untreated cells (control) were observed to be uniformly green with a normal structure and very low apoptosis and necrosis. (B) and (C): Treated cells at a concentration of 10 and 25 μg/mL of Ab-AuNPs demonstrated early and late apoptosis and necrosis. Early apoptosis features include orange-green amongst the fragmented DNA and chromatin condensation. Late apoptosis appears as dark orange, and bright red necrosis is obvious. Cells are introduced as the viable cell (V), early apoptotic cell (EA), late apoptotic cell (LA), and necrotic cell (N) using arrows. The values are shown as mean ± SD (n = 3). (200× magnification & 400× magnification).

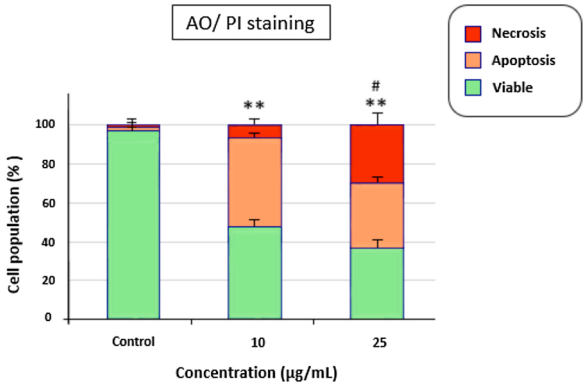

Fig. 9. Assessment of the percentage of viable, apoptotic, and necrotic NTERA-2 cells treated with concentrations of A) 0, B) 10, and C) 25 μg/mL of Ab-AuNPs for 24 h calculated from AO/PI staining. Compared to the control group (** $p <$ 0.01), comparing the two concentrations with each other (* $p < 0.05$).

changes in the expression of genes, which in part causes new alterations in the cell [83]. The key regulatory process of apoptosis includes death receptors, caspases' activation, Bax gene expression, and Bcl2 gene expression control [84]. In the apoptosis process, caspases are activated and act on their substrates, causing biological and structural changes in apoptotic cells. These enzymes are responsible for initiating the hallmarks and the execution phase of apoptosis, including DNA fragmentation, membrane blebbing, and cell shrinkage. Caspase-3 and caspase-9 have been recognized as key regulators of programmed cell death; therefore, the evaluation of caspase activity as a biochemical marker of

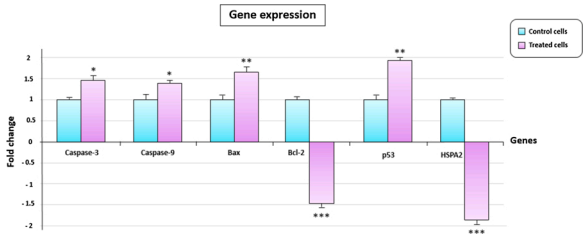

Fig. 10. RT-PCR analysis of caspase-3, caspase-9, Bax, Bcl2, p53, and HSPA2 mRNA expression in NTERA-2 cells, untreated cells as the control and cells treated with Ab-AuNPs (IC50 value) for 24 h. *$p <$ 0.05, **$p <$ 0.01 and ***$p <$ 0.001 were considered as statistically significant vs. control.

apoptosis is warranted [85].

Herein, the expression levels of both caspase-3 and caspase-9 were higher in treated cells compared with untreated cells at respectively 1.46- and 1.39-fold changes ($p < 0.05$) (Fig. 10), indicating that apoptosis was mediated through caspase cascade. The results revealed higher gene expression levels of Bax (1.65-fold change) and lower gene expression of Bcl2 (1.48-fold change) in cells exposed to Ab-AuNPs compared to untreated cells ($p < 0.01$ and $p<0.001$, respectively) (Fig. 10).

Based on the findings, an inverse relationship was observed between the anti-apoptotic Bcl2 and the pro-apoptotic Bax gene expression. The inhibitory effects of Ab-AuNPs on Bcl2 gene expression were significant with a remarkable reduction. Moreover, Bax gene expression considerably increased after cell treatment with nanoparticles. The expression levels of Bax and Bcl2 genes could be differently controlled by Ab-AuNPs, which suggests that a balance in the expression of these genes and their related proteins may play a role in controlling the process of apoptosis. Bax and Bcl_2 belong to a multi-gene family of proteins with homodimer and heterodimer structures. Bax induces programmed cell death and has an opposite function to that of Bcl_2. Anti-apoptotic proteins (Bcl2) are located extensively on the surface of the mitochondrial outer membrane, the endoplasmic reticulum, and the nuclear membrane, preserving the entire membrane. Tumors can inhibit apoptosis by enhancing anti-apoptotic regulator expression (Bcl2) and reducing apoptotic factors such as Bim, Bax, and Puma [86]. The results of this study confirmed the findings of previous studies that identified the function of apoptotic factors, such as caspases, Bax, and Bcl2 [87–89]. Ritwik Maity et al. stated that ROS production and mitochondrial depolarization stimulation by *theaflavin* conjugated AuNPs (AuNP@TfQ) on human ovarian cancer cells altered the Bax/Bcl2 proportion and ultimately activated the apoptotic factors in the treated PA-1 cells. A major up-regulation of the pro-apoptotic indicators (Bax, Bad, BID, and BIM) was shown in their findings, whereas the down-regulation of anti-apoptotic indicators (Bcl2 and Bcl-w) was observed. Additionally, the results demonstrated that the caspase family (caspase-3 and caspase-8) was upregulated, and the most likely justification for apoptosis induction was caspase-mediated cell death [90].

The tumor suppresser gene p53 played a key role in apoptosis stimulation and was implicated in cancer medical care. However, over 50 % of all tumors possess deactivated p53, and it is considered the most accepted cause of drug resistance and poor chemotherapeutic outcomes [91]. *In vitro* and *in vivo* studies revealed the return of p53 gene activity in several cancer cells, resulting in apoptosis induction [92].

Herein, p53 expression was investigated in treated and untreated

cells to estimate the molecular mechanism of NTERA-2 cells in the existence of Ab-AuNPs. In treated cells, a significant up-regulation (1.92-fold change, $p<0.01$) was observed in the expression of tumor suppressor gene p53 as compared to the control (Fig. 10). It has been stated that the elevated levels of p53 expression and DNA-damaging factors act synergistically to induce apoptosis and reverse the persistence in cancer cells [93]. Another study indicated that P53 and P53-downstream (P21 and P27) gene expression was significantly up-regulated in AuNP@TfQ-treated PA-1 cells [90].

P53 is a phosphoprotein transcription agent that controls the expression of more than 2500 target genes. It is involved in various cellular processes such as genome preservation, longevity, metabolism, and tumor suppressor [94]. Regarding the P53-dependent apoptotic transcriptional activity, this factor acts as a transcription agent for a set of pro-apoptotic proteins from the Bcl2 family (Puma Noxa Bid Bax), increasing the expression of these proteins and ultimately inducing mitochondrial permeability and the release of cytochrome c. Cytochrome c is essential for activating Apaf-1 and plays a vital role in activating caspases [95]. In a transcription-independent pathway, P53 directly targets mitochondria, binds to Bcl2 and Bcl-XL, and reduces their inhibitory effect on Bax and Bak proteins. Finally, it causes mitochondrial permeability and cytochrome c release [96]. The relationship between the high expression of this gene in testicular cancer cells and its sensitivity to chemotherapy and radiation therapy is significant for researchers. As noted earlier, after the cell DNA is damaged and the P53 gene expression level is increased, high levels of the gene in testicular cancer cells may make them prone to apoptosis [97]. Of course, other genes are also involved in apoptosis and produce high levels of BAX protein, an apoptotic booster protein in testicular cancer cells. However, these cells show very low levels of expression of the Bcl2 gene, a protein that weakens apoptosis [98].

Heat shock proteins (HSP) are intracellular protective proteins that contribute to the initial and re-folding and twisting of proteins. These proteins are highly expressed in response to stressful conditions such as heat, oxidative stress, and chemicals [99]. They also protect cell nuclei and lipid membranes from damage and prevent apoptosis, a fundamental and important cellular mechanism that allows cells to survive environmental damage [100]. HSPs play a dual and opposite role against cancer cells. On the one hand, it contributes to the growth and survival of cancer cells due to its involvement in the folding process or the collection of proteins and factors involved in cell proliferation, thereby enhancing the resistance of cancer cells. On the other hand, it stimulates the innate immune mechanism and mutually increases cancer antigens for lymphocytes, thus contributing to the body's immunity against cancer [101]. According to previous studies, these proteins are associated with many tumor antigenic peptides and are their carriers. They also play a role in the formation of immunological complexes (peptide–HSP complexes) as protective molecules. The immunological function of HSP became apparent when the HSPs obtained from the tumor provided active and effective immunity against it [102]. Therefore, it is essential to estimate the expression of this gene in treated cancer cells.

Herein, the HSPA2 expression was dramatically decreased in NTERA-2 cells treated with Ab-AuNPs compared to the untreated cells (1.84-fold change, $p<0.001$) (Fig. 10). Decreased HSPA2 expression by Ab-AuNPs treatment may have reduced meiosis for the period cell cycle, prompted DNA damage and, as a result, inhibited cancer cells' growth. HSPA2 (formerly HSP70-2) is a member of the genes related to the mitochondria in the cell and greatly contributes to meiosis improvement in cell differentiation. HSP70-2 may support DNA fixation proteins in cancer cells, and its deficiency induces DNA destruction, growth arrest, and cell death [103]. Jäättelä et al. demonstrated that Hsp70-2 expression was significantly increased in a subset of human breast cancer samples, and that its deficiency caused a striking anti-proliferative reaction unique to cancer cells [104].

4. Conclusion

In recent years, biology and nanotechnology researchers have paid special attention to nanoparticles' structures, shapes, combinations, and unique physicochemical properties for medical treatment protocols, pharmaceutical products, and drug delivery. Herein, for the first time, it was shown that the *A. biebersteinii* aqueous flower extract acts as a capping/reducing factor in AuNP biosynthesis. This synthesis method is very rapid, biocompatible, and cost-effective. The characterization results confirmed the spherical shape of the smallest Ab-AuNPs with a particle size of 2–30 nm and a mean diameter of 8 nm. The toxicity study of Ab-AuNPs on the testicular cancer cell line (NTERA-2) showed dose-dependent toxicity. The results suggested a correlation between Ab-AuNP-induced apoptosis, caspases 3/9 gene expression, and Bax and Bcl2 family proteins' expression in the NTERA-2 cell lines. It is also concluded that the Ab-AuNP-induced apoptotic pathway in these cells might be p53-dependent, and the HSPA2 gene expression could induce apoptosis via an associated signal pathway. Overall, the coordinate efficiency of these molecules is essential for regulating cell life and death.

The synthesized AuNPs demonstrate multifunctional properties for a more effective cancer treatment that can be easily transferred to the clinic. Additionally, fundamental investigations are warranted to identify the molecular interactions of NPs with their target cells. An important problem before the vaster application of AuNPs in the clinic, i.e., cytotoxicity, must be attentively tested. Although AuNPs are reported to be inherently nontoxic, it is essential to assess the toxicity of the NP core and its capping ligands. By tagging NPs with functional molecules, the efficacy of anticancer therapeutics can be dramatically enhanced. The present research highlighted the utility of nanoscale materials to promote the apoptotic properties of AuNPs against testicular cancer cells. It is suggested that the synthesized Ab-AuNPs be used in medicine, particularly for cancer treatment. It is also essential to explore biofabricated NPs as a potential and practical source of unique anticancer factors. More studies are warranted to disclose novel molecular targets that are solely expressed in the tumor microenvironment to aid the targeting of NP-based therapy. In the future, research should focus on the cellular and molecular mechanism of Ab-AuNPs in *in vivo* models to fill in this knowledge gap. The evaluation of the effects of Ab-AuNPs in the diagnosis and treatment of various cancers is also recommended. Hence, more progress in Ab-AuNPs testing (*in vitro* and *in vivo*) is required to guarantee patient safety, including the improvement of standard testing resources and procedures. The nanoparticles' transference, accumulation, and fate inside the human body must be systematically studied before their use can be authorized as an anticancer drug. In conclusion, the fabricated Ab-AuNP is a huge step forward and a promising treatment strategy for the treatment of cancers, especially testicular cancer.

Declaration of Competing Interest

The authors report no declarations of interest.

Acknowledgments

This research was financially supported by the Mashhad University of Medical Sciences (grant number: 971102) and Omid Cancer Center.

References

[1] M.E.T. Yazdi, M. Darroudi, M.S. Amiri, H.A. Hosseini, F. Nourbakhsh, M. Mashreghi, M. Farjadi, S.M.M. Kouhi, S.H. Mousavi, Anticancer, antimicrobial, and dye degradation activity of biosynthesised silver nanoparticle using Artemisia kopetdaghensis, Micro Nano Lett. 15 (14) (2020) 1046–1050, https://doi.org/10.1049/mnl.2020.0387.

[2] A. Es-haghi, M.E. Taghavizadeh Yazdi, M. Sharifalhoseini, M. Baghani, E. Yousefi, A. Rahdar, F. Baino, Application of response surface methodology for optimizing the therapeutic activity of ZnO nanoparticles biosynthesized from Aspergillus niger, Biomimetics 6 (2) (2021) 34.

[3] S. Nazir, T. Hussain, A. Ayub, U. Rashid, A.J. MacRobert, Nanomaterials in combating cancer: therapeutic applications and developments, Nanomed. Nanotechnol. Biol. Med. 10 (1) (2014) 19–34.

[4] N. Lakpour, K. Saliminejad, R. Ghods, M. Reza Sadeghi, A. Pilatz, F. Khosravi, Z. Madjd, Potential biomarkers for testicular germ cell tumour: risk assessment, diagnostic, prognostic and monitoring of recurrence, Andrologia 53 (4) (2021), e13998.

[5] L. De Toni, I. Šabovic, I. Cosci, M. Ghezzi, C. Foresta, A. Garolla, Testicular cancer: genes, environment, hormones, Front. Endocrinol. (Lausanne) 10 (2019) 408.

[6] M. Ashna, A. Es-Haghi, M. Karimi Noghondar, D. Al Amara, M.E.T. Yazdi, Greener synthesis of cerium oxide nanoemulsion using pollen grains of Brassica napus and evaluation of its antitumour and cytotoxicity properties, Mater. Technol. (2020) 1–8.

[7] M.R. Hashemzadeh, M.E.T. Yazdi, M.S. Amiri, S.H. Mousavi, Stem cell therapy in the heart: biomaterials as a key route, Tissue Cell (2021), 101504.

[8] M.E.T. Yazdi, F. Nourbakhsh, M. Mashreghi, S.H. Mousavi, Ultrasound-based synthesis of ZnO· Ag 2 O 3 nanocomposite: characterization and evaluation of its antimicrobial and anticancer properties, Res. Chem. Intermed. (2021) 1–12.

[9] M. Zarei, E. Karimi, E. Oskoueian, A. Es-Haghi, M.E.T. Yazdi, Comparative study on the biological effects of sodium citrate-based and apigenin-based synthesized silver nanoparticles, Nutr. Cancer (2020) 1–9.

[10] M. Darroudi, M.E.T. Yazdi, M.S. Amiri, Plant-Mediated Biosynthesis of Nanoparticles, 21st Century Nanoscience–A Handbook, CRC Press, 2020, pp. 1-1–1-18.

[11] H. Sharifan, X. Ma, Foliar application of Zn agrichemicals affects the bioavailability of arsenic, cadmium and micronutrients to rice (Oryza sativa L.) in flooded paddy soil, Agriculture 11 (6) (2021) 505.

[12] A.B.-K. Seyed Mousa Mousavi-kouhi, Mohammad Sadegh Amiri, Mohammad Mashreghi, Mohammad Ehsan Taghavizadeh Yazdi, Silver-zinc oxide nanocomposite: from synthesis to antimicrobial and anticancer properties, Ceram. Int. 47 (15) (2021) 21490–21497, https://doi.org/10.1016/j.ceramint.2021.04.160.

[13] M.E. Taghavizadeh Yazdi, A. Hamidi, M.S. Amiri, R. Kazemi Oskuee, H. A. Hosseini, A. Hashemzadeh, M. Darroudi, Eco-friendly and plant-based synthesis of silver nanoparticles using Allium giganteum and investigation of its bactericidal, cytotoxicity, and photocatalytic effects, Mater. Technol. 34 (8) (2019) 490–497.

[14] K. Saravanakumar, A. Sathiyaseelan, A.V.A. Mariadoss, X. Hu, K. Venkatachalam, M.-H. Wang, Nucleolin targeted delivery of aptamer tagged Trichoderma derived crude protein coated gold nanoparticles for improved cytotoxicity in cancer cells, Process. Biochem. 102 (2021) 325–332.

[15] M.E.T. Yazdi, J. Khara, H.R. Sadeghnia, S.E. Bahabadi, M. Darroudi, Biosynthesis, characterization, and antibacterial activity of silver nanoparticles using Rheum turkestanicum shoots extract, Res. Chem. Intermed. 44 (2) (2018) 1325–1334.

[16] M. Uzma, N. Sunayana, V.B. Raghavendra, C.S. Madhu, R. Shanmuganathan, K. Brindhadevi, Biogenic synthesis of gold nanoparticles using Commiphora wightii and their cytotoxic effects on breast cancer cell line (MCF-7), Process. Biochem. 92 (2020) 269–276.

[17] S. Ningaraju, U. Munawer, V.B. Raghavendra, K.S. Balaji, G. Melappa, K. Brindhadevi, A. Pugazhendhi, Chaetomium globosum extract mediated gold nanoparticle synthesis and potent anti-inflammatory activity, Anal. Biochem. 612 (2021), 113970.

[18] U. Munawer, V.B. Raghavendra, S. Ningaraju, K.L. Krishna, A.R. Ghosh, G. Melappa, A. Pugazhendhi, Biofabrication of gold nanoparticles mediated by the endophytic Cladosporium species: photodegradation, in vitro anticancer activity and in vivo antitumor studies, Int. J. Pharm. 588 (2020), 119729.

[19] K. Govindaraju, R. Vasantharaja, K.U. Suganya, S. Anbarasu, K. Revathy, A. Pugazhendhi, D. Karthickeyan, G. Singaravelu, Unveiling the anticancer and antimycobacterial potentials of bioengineered gold nanoparticles, Process. Biochem. 96 (2020) 213–219.

[20] S. Senapati, A. Syed, S. Moeez, A. Kumar, A. Ahmad, Intracellular synthesis of gold nanoparticles using alga Tetraselmis kochinensis, Mater. Lett. 79 (2012) 116–118.

[21] H.M. Azzazy, M.M. Mansour, T.M. Samir, R. Franco, Gold nanoparticles in the clinical laboratory: principles of preparation and applications, Clin. Chem. Lab. Med. (CCLM) 50 (2) (2012) 193–209.

[22] M.E. Taghavizadeh Yazdi, S. Nazarnezhad, S.H. Mousavi, M. Sadegh Amiri, M. Darroudi, F. Baino, S. Kargozar, Gum tragacanth (GT): a versatile biocompatible material beyond borders, Molecules 26 (6) (2021) 1510.

[23] A. Hamidi, M.E.T. Yazdi, M.S. Amiri, H.A. Hosseini, M. Darroudi, Biological synthesis of silver nanoparticles in Tribulus terrestris L. extract and evaluation of their photocatalyst, antibacterial, and cytotoxicity effects, Res. Chem. Intermed. 45 (5) (2019) 2915–2925.

[24] E.M. Bolbanabad, M. Ashengroph, F. Darvishi, Development and evaluation of different strategies for the clean synthesis of silver nanoparticles using Yarrowia lipolytica and their antibacterial activity, Process. Biochem. 94 (2020) 319–328.

[25] M.S. Amiri, V. Mohammadzadeh, M.E.T. Yazdi, M. Barani, A. Rahdar, G.Z. Kyzas, Plant-based gums and mucilages applications in pharmacology and nanomedicine: a review, Molecules 26 (6) (2021) 1770.

[26] M. Modarres, M.E.T. Yazdi, Elicitation improves phenolic acid content and antioxidant enzymes activity in salvia leriifolia cell cultures, Iran. J. Sci. Technol. Trans. A: Sci. (2021) 1–7.

[27] M.E.T. Yazdi, M. Modarres, M.S. Amiri, M. Darroudi, Phyto-synthesis of silver nanoparticles using aerial extract of Salvia leriifolia Benth and evaluation of their antibacterial and photo-catalytic properties, Res. Chem. Intermed. 45 (3) (2019) 1105–1116.

[28] F. Javadi, M.E.T. Yazdi, M. Baghani, A. Es-haghi, Biosynthesis, characterization of cerium oxide nanoparticles using Ceratonia siliqua and evaluation of antioxidant and cytotoxicity activities, Mater. Res. Express 6 (6) (2019), 065408.

[29] M.E.T. Yazdi, M.S. Amiri, H.A. Hosseini, R.K. Oskuee, H. Mosawee, K. Pakravanan, M. Darroudi, Plant-based synthesis of silver nanoparticles in Handelia trichophylla and their biological activities, Bull. Mater. Sci. 42 (4) (2019) 155.

[30] K. Atacan, CuFe2O4/reduced graphene oxide nanocomposite decorated with gold nanoparticles as a new electrochemical sensor material for L-cysteine detection, J. Alloys Compd. 791 (2019) 391–401.

[31] A.D. Dwivedi, K. Gopal, Biosynthesis of silver and gold nanoparticles using Chenopodium album leaf extract, Colloids Surf. A Physicochem. Eng. Asp. 369 (1) (2010) 27–33.

[32] M.S. Amiri, M.E.T. Yazdi, M. Rahnama, Medicinal plants and phytotherapy in Iran: glorious history, current status and future prospects, Plant Sci. Today 8 (1) (2021) 95–111.

[33] H. Sharifan, J. Moore, X. Ma, Zinc oxide (ZnO) nanoparticles elevated iron and copper contents and mitigated the bioavailability of lead and cadmium in different leafy greens, Ecotoxicol. Environ. Saf. 191 (2020), 110177.

[34] A. Motavalizadehkakhky, A. Shafaghat, H.A. Zamani, H. Akhlaghi, M. Mohammadhosseini, J. Mehrzad, Z. Ebrahimi, Compositions and the in vitro antimicrobial activities of the essential oils and extracts of two Achillea species from Iran, J. Med. Plants Res. 7 (19) (2013) 1280–1292.

[35] J.Z. Al-Kalaldeh, R. Abu-Dahab, F.U. Afifi, Volatile oil composition and antiproliferative activity of Laurus nobilis, Origanum syriacum, Origanum vulgare, and Salvia triloba against human breast adenocarcinoma cells, Nutr. Res. 30 (4) (2010) 271–278.

[36] B. Salehi, Z. Selamoglu, M. Sevindik, N.M. Fahmy, E. Al-Sayed, M. El-Shazly, B. Csupor-Löffler, D. Csupor, S.E. Yazdi, J. Sharifi-Rad, Achillea spp.: a comprehensive review on its ethnobotany, phytochemistry, phytopharmacology and industrial applications, Cell. Mol. Biol. 66 (4) (2020) 78–103.

[37] S.B. Nimse, D. Pal, Free radicals, natural antioxidants, and their reaction mechanisms, RSC Adv. 5 (35) (2015) 27986–28006.

[38] J.R. Nakkala, R. Mata, E. Bhagat, S.R. Sadras, Green synthesis of silver and gold nanoparticles from Gymnema sylvestre leaf extract: study of antioxidant and anticancer activities, J. Nanoparticle Res. 17 (3) (2015) 1–15.

[39] M. Nishikimi, N.A. Rao, K. Yagi, The occurrence of superoxide anion in the reaction of reduced phenazine methosulfate and molecular oxygen, Biochem. Biophys. Res. Commun. 46 (2) (1972) 849–854.

[40] A. Es-haghi, F. Javadi, M.E.T. Yazdi, M.S. Amiri, The expression of antioxidant genes and cytotoxicity of biosynthesized cerium oxide nanoparticles against hepatic carcinoma cell line, Avicenna J. Med. Biochem. 7 (1) (2019) 16–20.

[41] J. Baharara, T. Ramezani, A. Divsalar, M. Mousavi, A. Seyedarabi, Induction of apoptosis by green synthesized gold nanoparticles through activation of caspase-3 and 9 in human cervical cancer cells, Avicenna J. Med. Biotechnol. 8 (2) (2016) 75.

[42] M. Shafagh, F. Rahmani, N. Delirezh, CuO nanoparticles induce cytotoxicity and apoptosis in human K562 cancer cell line via mitochondrial pathway, through reactive oxygen species and P53, Iran. J. Basic Med. Sci. 18 (10) (2015) 993.

[43] J. Baharara, N. Hosseini, T.R. Farzin, Extremely low frequency electromagnetic field sensitizes cisplatin-resistant human ovarian adenocarcinoma cells via P53 activation, Cytotechnology 68 (4) (2016) 1403–1413.

[44] R.A. Mahmoudian, M.M. Forghanifard, Crosstalk between MEIS1 and markers of different cell signaling pathways in esophageal squamous cell carcinoma, Mol. Biol. Rep. 47 (5) (2020) 3439–3448.

[45] M. Bindhu, M. Umadevi, Silver and gold nanoparticles for sensor and antibacterial applications, Spectrochim. Acta A Mol. Biomol. Spectrosc. 128 (2014) 37–45.

[46] M. Bindhu, P.V. Rekha, T. Umamaheswari, M. Umadevi, Antibacterial activities of Hibiscus cannabinus stem-assisted silver and gold nanoparticles, Mater. Lett. 131 (2014) 194–197.

[47] A.K. Singh, R. Tiwari, V.K. Singh, P. Singh, S.R. Khadim, U. Singh, V. Srivastava, S. Hasan, R. Asthana, Green synthesis of gold nanoparticles from Dunaliella salina, its characterization and in vitro anticancer activity on breast cancer cell line, J. Drug Deliv. Sci. Technol. 51 (2019) 164–176.

[48] J.K. Andeani, H. Kazemi, S. Mohsenzadeh, A. Safavi, Biosynthesis of gold nanoparticles using dried flowers extract of Achillea wilhelmsii plant, Dig. J. Nanomater. Bios. 6 (2011) 1011–1017.

[49] J.Y. Song, H.-K. Jang, B.S. Kim, Biological synthesis of gold nanoparticles using Magnolia kobus and Diopyros kaki leaf extracts, Process. Biochem. 44 (10) (2009) 1133–1138.

[50] M. Noruzi, D. Zare, K. Khoshnevisan, D. Davoodi, Rapid green synthesis of gold nanoparticles using Rosa hybrida petal extract at room temperature, Spectrochim. Acta A Mol. Biomol. Spectrosc. 79 (5) (2011) 1461–1465.

[51] T. Prathna, N. Chandrasekaran, A.M. Raichur, A. Mukherjee, Biomimetic synthesis of silver nanoparticles by Citrus limon (lemon) aqueous extract and theoretical prediction of particle size, Colloids Surf. B Biointerfaces 82 (1) (2011) 152–159.

[52] S.P. Chandran, M. Chaudhary, R. Pasricha, A. Ahmad, M. Sastry, Synthesis of gold nanotriangles and silver nanoparticles using Aloevera plant extract, Biotechnol. Prog. 22 (2) (2006) 577–583.

[53] M.M. Khalil, E.H. Ismail, F. El-Magdoub, Biosynthesis of Au nanoparticles using olive leaf extract: 1st nano updates, Arab. J. Chem. 5 (4) (2012) 431–437.

[54] M.E.T. Yazdi, J. Khara, M.R. Housaindokht, H.R. Sadeghnia, S.E. Bahabadi, M. S. Amiri, H. Mosawee, D. Taherzadeh, M. Darroudi, Role of Ribes khorassanicum in the biosynthesis of AgNPs and their antibacterial properties, IET Nanobiotechnol. 13 (2) (2018) 189–192.
[55] P. Ragavendran, D. Sophia, C. Arul Raj, V. Gopalakrishnan, Functional group analysis of various extracts of Aerva lanata (L.,) by ftir spectrum, Pharmacologyonline 1 (2011) 358–364.
[56] R. Ashokkumar, M. Ramaswamy, Phytochemical screening by FTIR spectroscopic analysis of leaf extracts of selected Indian Medicinal plants, J. Curr. Microbiol. Appl. Sci. 3 (1) (2014) 395–406.
[57] D. Jain, H.K. Daima, S. Kachhwaha, S. Kothari, Synthesis of plant-mediated silver nanoparticles using papaya fruit extract and evaluation of their anti microbial activities, Dig. J. Nanomater. Biostruct. 4 (3) (2009) 557–563.
[58] C. Singh, R.K. Baboota, P.K. Naik, H. Singh, Biocompatible Synthesis of Silver and Gold Nanoparticles Using Leaf Extract of Dalbergia sissoo, 2012.
[59] A. Vágó, G. Szakacs, G. Sáfrán, R. Horvath, B. Pécz, I. Lagzi, One-step green synthesis of gold nanoparticles by mesophilic filamentous fungi, Chem. Phys. Lett. 645 (2016) 1–4.
[60] Y.-C. Yeh, B. Creran, V.M. Rotello, Gold nanoparticles: preparation, properties, and applications in bionanotechnology, Nanoscale 4 (6) (2012) 1871–1880.
[61] A.I. Usman, A.A. Aziz, O.A. Noqta, Green sonochemical synthesis of gold nanoparticles using palm oil leaves extracts, Mater. Today Proc. 7 (2019) 803–807.
[62] M. Aguilar, F. Mares-Briones, S. Borjas-García, G. Rosas, Green synthesis of gold nanoparticles using Origanum vulgare, Microsc. Microanal. 25 (S2) (2019) 2378–2379.
[63] S.S. Shankar, A. Ahmad, R. Pasricha, M. Sastry, Bioreduction of chloroaurate ions by geranium leaves and its endophytic fungus yields gold nanoparticles of different shapes, J. Mater. Chem. 13 (7) (2003) 1822–1826.
[64] J.Y. Song, B.S. Kim, Rapid biological synthesis of silver nanoparticles using plant leaf extracts, Bioprocess Biosyst. Eng. 32 (1) (2009) 79.
[65] M.E.T. Yazdi, M.S. Amiri, S. Akbari, M. Sharifalhoseini, F. Nourbakhsh, M. Mashreghi, M.R. Abbasi, M. Modarres, A. Es-haghi, Green synthesis of silver nanoparticles using Helichrysum graveolens for biomedical applications and wastewater treatment, BioNanoScience (2020) 1–7.
[66] C. Sun, R. Qu, H. Chen, C. Ji, C. Wang, Y. Sun, B. Wang, Degradation behavior of chitosan chains in the 'green'synthesis of gold nanoparticles, Carbohydr. Res. 343 (15) (2008) 2595–2599.
[67] J. Kasthuri, K. Kathiravan, N. Rajendiran, Phyllanthin-assisted biosynthesis of silver and gold nanoparticles: a novel biological approach, J. Nanoparticle Res. 11 (5) (2009) 1075–1085.
[68] K. Huang, H. Ma, J. Liu, S. Huo, A. Kumar, T. Wei, X. Zhang, S. Jin, Y. Gan, P. C. Wang, Size-dependent localization and penetration of ultrasmall gold nanoparticles in cancer cells, multicellular spheroids, and tumors in vivo, ACS Nano 6 (5) (2012) 4483–4493.
[69] T. Yazdi, M. Ehsan, M.R. Housaindokht, H.R. Sadeghnia, S. Esmaeilzadeh Bahabadi, M.S. Amiri, M. Darroudi, Assessment of phytochemical components and antioxidant activity of Rheum turkestanicum Janisch, Stud. Med. Sci. 31 (2) (2020) 75–81.
[70] Q. Liu, F. Wu, Y. Chen, S.T. Alrashood, S.A. Alharbi, Anti-human colon cancer properties of a novel chemotherapeutic supplement formulated by gold nanoparticles containing Allium sativum L. leaf aqueous extract and investigation of its cytotoxicity and antioxidant activities, Arab. J. Chem. 14 (4) (2021), 103039.
[71] J.R. Nakkala, R. Mata, E. Bhagat, S.R. Sadras, Green synthesis of silver and gold nanoparticles from Gymnema sylvestre leaf extract: study of antioxidant and anticancer activities, J. Nanoparticle Res. 17 (3) (2015) 151.
[72] H. Bao, Q. Zhang, H. Xu, Z. Yan, Effects of nanoparticle size on antitumor activity of 10-hydroxycamptothecin-conjugated gold nanoparticles: in vitro and in vivo studies, Int. J. Nanomedicine 11 (2016) 929.
[73] A. Sani, C. Cao, D. Cui, Toxicity of gold nanoparticles (AuNPs): a review, Biochem. Biophys. Rep. 26 (2021), 100991.
[74] M. Enea, E. Pereira, J. Costa, M.E. Soares, D.D. da Silva, M. de Lourdes Bastos, H. F. Carmo, Cellular uptake and toxicity of gold nanoparticles on two distinct hepatic cell models, Toxicol. In Vitro 70 (2021), 105046.
[75] M.P. Patil, X. Jin, N.C. Simeon, J. Palma, D. Kim, D. Ngabire, N.-H. Kim, N. H. Tarte, G.-D. Kim, Anticancer activity of Sasa borealis leaf extract-mediated gold nanoparticles, Artif. Cells Nanomed. Biotechnol. 46 (1) (2018) 82–88.
[76] J. Chen, Y. Li, G. Fang, Z. Cao, Y. Shang, S. Alfarraj, S.A. Alharbi, J. Li, S. Yang, X. Duan, Green synthesis, characterization, cytotoxicity, antioxidant, and anti-human ovarian cancer activities of Curcumae kwangsiensis leaf aqueous extract green-synthesized gold nanoparticles, Arab. J. Chem. 14 (3) (2021), 103000.
[77] S. Li, F.A. Al-Misned, H.A. El-Serehy, L. Yang, Green synthesis of gold nanoparticles using aqueous extract of Mentha Longifolia leaf and investigation of its anti-human breast carcinoma properties in the in vitro condition, Arab. J. Chem. 14 (2) (2021), 102931.
[78] C. Krishnaraj, P. Muthukumaran, R. Ramachandran, M. Balakumaran, P. Kalaichelvan, Acalypha indica Linn: biogenic synthesis of silver and gold nanoparticles and their cytotoxic effects against MDA-MB-231, human breast cancer cells, Biotechnol. Rep. 4 (2014) 42–49.
[79] M.V. Park, A.M. Neigh, J.P. Vermeulen, L.J. de la Fonteyne, H.W. Verharen, J. J. Briedé, H. van Loveren, W.H. de Jong, The effect of particle size on the cytotoxicity, inflammation, developmental toxicity and genotoxicity of silver nanoparticles, Biomaterials 32 (36) (2011) 9810–9817.
[80] D.V. Krysko, K. D'Herde, P. Vandenabeele, Clearance of apoptotic and necrotic cells and its immunological consequences, Apoptosis 11 (10) (2006) 1709–1726.
[81] L. Wang, J. Xu, Y. Yan, H. Liu, T. Karunakaran, F. Li, Green synthesis of gold nanoparticles from Scutellaria barbata and its anticancer activity in pancreatic cancer cell (PANC-1), Artif. Cells Nanomed. Biotechnol. 47 (1) (2019) 1617–1627.
[82] M. Vairavel, E. Devaraj, R. Shanmugam, An eco-friendly synthesis of Enterococcus sp.–mediated gold nanoparticle induces cytotoxicity in human colorectal cancer cells, Environ. Sci. Pollut. Res. - Int. 27 (8) (2020) 8166–8175.
[83] Y. Cai, J. Lu, F. Tang, Overexpression of MICAL2, a novel tumor-promoting factor, accelerates tumor progression through regulating cell proliferation and EMT, J. Cancer 9 (3) (2018) 521.
[84] S.H. Mousavi, J. Tavakkol-Afshari, A. Brook, I. Jafari-Anarkooli, Role of caspases and Bax protein in saffron-induced apoptosis in MCF-7 cells, Food Chem. Toxicol. 47 (8) (2009) 1909–1913.
[85] Z. Cheng, Z. Zhang, Y. Han, J. Wang, Y. Wang, X. Chen, Y. Shao, Y. Cheng, W. Zhou, X. Lu, A review on anti-cancer effect of green tea catechins, J. Funct. Foods 74 (2020), 104172.
[86] Z. Liu, R. Sun, W. Lü, C. Dang, Y. Song, C. Wang, X. Zhang, L. Han, H. Cheng, W. Gao, The-938A/A genotype of BCL2 gene is associated with esophageal cancer, Med. Oncol. 29 (4) (2012) 2677–2683.
[87] J. Baharara, F. Namvar, T. Ramezani, M. Mousavi, R. Mohamad, Silver nanoparticles biosynthesized using Achillea biebersteinii flower extract: apoptosis induction in MCF-7 cells via caspase activation and regulation of Bax and Bcl-2 gene expression, Molecules 20 (2) (2015) 2693–2706.
[88] G. Ghavami, S. Sardari, M.A. Shokrgozar, Anticancerous potentials of Achillea species against selected cell lines, J. Med. Plants Res. 4 (22) (2010) 2411–2417.
[89] C. Krishnaraj, E. Jagan, R. Ramachandran, S. Abirami, N. Mohan, P. Kalaichelvan, Effect of biologically synthesized silver nanoparticles on Bacopa monnieri (Linn.) Wettst. plant growth metabolism, Process. Biochem. 47 (4) (2012) 651–658.
[90] R. Maity, M. Chatterjee, A. Banerjee, A. Das, R. Mishra, S. Mazumder, N. Chanda, Gold nanoparticle-assisted enhancement in the anti-cancer properties of theaflavin against human ovarian cancer cells, Mater. Sci. Eng. C 104 (2019), 109909.
[91] M.J. Duffy, N.C. Synnott, P.M. McGowan, J. Crown, D. O'Connor, W. M. Gallagher, p53 as a target for the treatment of cancer, Cancer Treat. Rev. 40 (10) (2014) 1153–1160.
[92] T. Ramezani, M. Nabiuni, J. Baharara, K. Parivar, F. Namvar, Sensitization of resistance ovarian cancer cells to cisplatin by biogenic synthesized silver nanoparticles through p53 activation, Iran. J. Pharm. Res.: IJPR 18 (1) (2019) 222.
[93] M.M. Khalil, E.H. Ismail, K.Z. El-Baghdady, D. Mohamed, Green synthesis of silver nanoparticles using olive leaf extract and its antibacterial activity, Arab. J. Chem. 7 (6) (2014) 1131–1139.
[94] K. Pappas, J. Xu, S. Zairis, L. Resnick-Silverman, F. Abate, N. Steinbach, S. Ozturk, L.H. Saal, T. Su, P. Cheung, p53 maintains baseline expression of multiple tumor suppressor genes, Mol. Cancer Res. 15 (8) (2017) 1051–1062.
[95] E.M. Kim, C.-H. Jung, J. Kim, S.-G. Hwang, J.K. Park, H.-D. Um, The p53/p21 complex regulates cancer cell invasion and apoptosis by targeting Bcl-2 family proteins, Cancer Res. 77 (11) (2017) 3092–3100.
[96] H.-Y. Lee, S.-H. Oh, Autophagy-mediated cytoplasmic accumulation of p53 leads to apoptosis through DRAM-BAX in cadmium-exposed human proximal tubular cells, Biochem. Biophys. Res. Commun. 534 (2021) 128–133.
[97] J. Lobo, M.A. Alzamora, R. Guimarães, M. Cantante, P. Lopes, I. Braga, J. Maurício, C. Jerónimo, R. Henrique, p53 and MDM2 expression in primary and metastatic testicular germ cell tumors: association with clinical outcome, Andrology 8 (5) (2020) 1233–1242.
[98] O.O. Ojo, Expression of Bax and Bcl-2 apoptotic regulatory proteins in melphalan-induced spermatogenic dysfunction, Asian Pac. J. Health Sci. 7 (2) (2020) 7–11.
[99] F. Mobaraki, M. Seghatoleslam, A. Fazel, A. Ebrahimzadeh-Bideskan, Effects of MDMA (ecstasy) on apoptosis and heat shock protein (HSP70) expression in adult rat testis, Toxicol. Mech. Methods 28 (3) (2018) 219–229.
[100] M.E. Taghavizadeh Yazdi, M.S. Amiri, F. Nourbakhsh, M. Rahnama, F. Forouzanfar, S.H. Mousavi, Bio-indicators in cadmium toxicity: role of HSP27 and HSP70, Environ. Sci. Pollut. Res. - Int. 28 (2021) 26359–26379, https://doi.org/10.1007/s11356-021-13687-y.
[101] A.A. Asea, B.K. Pedersen, Heat Shock Proteins and Whole Body Physiology, Springer Science & Business Media, 2009.
[102] D.R. Ciocca, A.P. Arrigo, S.K. Calderwood, Heat shock proteins and heat shock factor 1 in carcinogenesis and tumor development: an update, Arch. Toxicol. 87 (1) (2013) 19–48.
[103] M.A. Vostakolaei, L. Hatami-Baroogh, G. Babaei, O. Molavi, S. Kordi, J. Abdolalizadeh, Hsp70 in cancer: a double agent in the battle between survival and death, J. Cell. Physiol. 236 (5) (2021) 3420–3444.
[104] M. Rohde, M. Daugaard, M.H. Jensen, K. Helin, J. Nylandsted, M. Jäättelä, Members of the heat-shock protein 70 family promote cancer cell growth by distinct mechanisms, Genes Dev. 19 (5) (2005) 570–582.